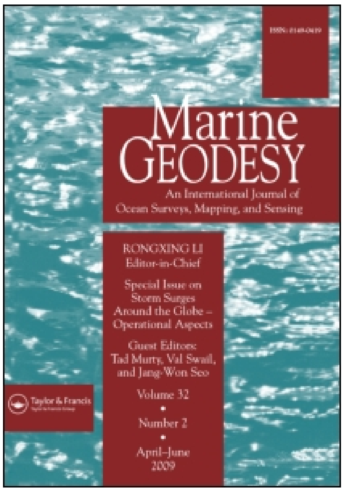

Marine Geodesy
Publication details, including instructions for authors and subscription information:
http://www.informaworld.com/smpp/title~content=t713657895

Validation of Jason-2 Altimeter Data by Waveform Retracking over California Coastal Ocean

Hyongki Lee[a]; C. K. Shum[a]; William Emery[b]; Stephane Calmant[cd]; Xiaoli Deng[e]; Chung-Yen Kuo[f]; Carolyn Roesler[b]; Yuchan Yi[a]
[a] Division of Geodetic Science, School of Earth Sciences, The Ohio State University, Columbus, Ohio, USA [b] Aerospace Engineering Sciences, University of Colorado, Boulder, Colorado, USA [c] Université de Toulouse, Toulouse, France [d] IRD, LEGOS, Toulouse, France [e] School of Engineering, The University of Newcastle, Callaghan, New South Wales, Australia [f] Department of Geomatics, National Cheng-Kung University, Tainan, Taiwan

Online publication date: 09 August 2010

To cite this Article Lee, Hyongki , Shum, C. K. , Emery, William , Calmant, Stephane , Deng, Xiaoli , Kuo, Chung-Yen , Roesler, Carolyn and Yi, Yuchan(2010) 'Validation of Jason-2 Altimeter Data by Waveform Retracking over California Coastal Ocean', Marine Geodesy, 33: 1, 304 — 316

To link to this Article: DOI: 10.1080/01490419.2010.488982
URL: http://dx.doi.org/10.1080/01490419.2010.488982

Marine Geodesy, 33(S1):304–316, 2010

ISSN: 0149-0419 print / 1521-060X online
DOI: 10.1080/01490419.2010.488982

Validation of Jason-2 Altimeter Data by Waveform Retracking over California Coastal Ocean

HYONGKI LEE,[1] C. K. SHUM,[1] WILLIAM EMERY,[2] STEPHANE CALMANT,[3,4] XIAOLI DENG,[5] CHUNG-YEN KUO,[6] CAROLYN ROESLER,[2] AND YUCHAN YI[1]

[1]Division of Geodetic Science, School of Earth Sciences, The Ohio State University, Columbus, Ohio, USA
[2]Aerospace Engineering Sciences, University of Colorado, Boulder, Colorado, USA
[3]Université de Toulouse, UPS (OMP-PCA), LEGOS, Toulouse, France
[4]IRD, LEGOS, Toulouse, France
[5]School of Engineering, The University of Newcastle, Callaghan, New South Wales, Australia
[6]Department of Geomatics, National Cheng-Kung University, Tainan, Taiwan

We validated Jason-2 satellite altimeter Sensor Geophysical Data Records (SGDR) by retracking 20-Hz radar waveforms over the California coastal ocean using cycles 7–34, corresponding to September 2008–June 2009. The performance of the ocean, ice, threshold, and modified threshold retrackers are examined using a reference geoid based on Earth Gravitational Model 2008 (EGM08). Over the shallow ocean (depth < 200 m), the modified threshold retracker, which is developed for noisy waveforms with preleading edge bump, outperforms the other retrackers. It is also shown that retracking can improve the precision of sea surface heights (SSHs) for areas beyond 2–5 km from the shore. Although the ocean retracker generally performs well over the deep ocean (depth > 200 m), the ocean-retracked SSHs from some of the cycles are found to be less precise when the waveforms do not conform to the Brown ocean model. We found that the retrackers developed for nonocean surfaces can improve the noisy ocean-retracked SSHs. Among the retrackers tested here, the ice retracker overall provides the most precise SSH estimates over the deep ocean in average using cycles 7–34 in the study region.

Keywords Jason-2, waveform retracking, California coastal ocean, modified threshold retracker

1. Introduction

Satellite radar altimetry is a mature technology to accurately measure the height and shape of the sea surface globally from space. It has been used to observe global ocean surface topography and its changes with unprecedented accuracy (about 2 cm root-mean-square (RMS) in sea surface heights (SSHs)) and resolutions (up to 50 km spatial scale and weekly

Received 23 December 2009; accepted 10 March 2010.
Address correspondence to Hyongki Lee, Division of Geodetic Science, School of Earth Sciences, The Ohio State University, 275 Mendenhall Laboratory, 125 South Oval Mall, Columbus, OH 43210. E-mail: lee.2444@osu.edu

temporal sampling) (Chelton et al. 2001; Shum et al. 2003). The observation principle of pulse-limited satellite radar altimetry is conceptually straightforward. It transmits an electromagnetic pulse to the sea surface and measures its two-way travel time when the return reflected from the instantaneous sea surface is received. The altimeter measures the range using an on-board tracker, which provides a time series of the received power distribution of the reflected pulse called the altimeter waveform. The two-way travel time represents the time for the midpoint of the pulse to return from the sea surface at nadir. Therefore, the altimeter determines the two-way travel time by identifying the half-power point on the leading edge of the waveform. The on-board tracker design is based on a Brown (1977) model of the return waveform, to align the return spectral waveform so that the half-power point of the leading edge is at a specified frequency. This tracking point corresponds to the gate 32 for 104-sample waveform of Jason-2 altimeter.

The SSH measurements from satellite radar altimetry in coastal region can be corrupted not only by less reliable geophysical and environmental corrections (Chelton et al. 2001) but also by the noisier radar returns from the generally rougher coastal sea states and simultaneous returns from reflective land and shallow water (Brooks et al. 1997; Deng and Featherstone 2006). Brooks et al. (1997) found that the land return influences TOPEX waveforms within distances of 4.1–34.8 km from coasts with the maximum near the East China Sea. Deng et al. (2002) observed that the waveforms from ERS-2 and Poseidon can be affected up to a maximum distance of 22 km off the Australian coast. Waveforms reflected from these affected coastal oceans do not conform to those over open oceans so that the on-board satellite tracking algorithm cannot accurately compute the range between the satellite and nadir surface, thus producing poorly estimated SSHs. Therefore, the altimeter range measurements over the coastal ocean must be corrected for the deviation of the midpoint of the leading edge from the tracking gate of the on-board tracker.

In recent years, a waveform retracking technique, which has been originally developed for altimeter measurements over ice sheets (Martin et al. 1983; Bamber 1994; Davis 1997), has extended its role into coastal ocean to reprocess the altimeter waveform data and improve the poorly estimated SSHs (e.g., Brooks et al. 1997; Anzenhofer et al. 1999; Deng and Featherstone 2006; Hwang et al. 2006; Bao et al. 2009). A recent review of waveform retracking methods can also be found in Lee et al. (2008a) and Gommenginger et al. (2009). The goal of this study is to determine the optimal retrackers among "ocean" and "ice" retrackers used in Jason-2 Sensor Geophysical Data Record (SGDR) and the original (Davis 1997) and modified threshold retrackers (Lee et al. 2008b) over the California shallow (depth $<$ 200 m) and deep (depth $>$ 200 m) oceans, respectively. While we perform retracking using the original and modified threshold retrackers, we directly use the ocean- and ice-retracked measurements available in the SGDR. The quality of ocean-retracked SSHs in the SGDR is also examined over the deep ocean. It should be noted that the purpose of this study is to focus on the above specific retrackers, not to evaluate all of the retrackers available in the scientific community.

2. Study Area and Data

The main objectives of the Jason-2 altimeter include the continuation of TOPEX/ Poseidon and Jason-1 records to observe global ocean topographic heights for more than a decade. Jason-2 satellite was launched in June 2008 and equipped with Poseidon-3 dual-frequency radar altimeter at Ku-band (13.6 GHz) and C-band (5.3 GHz) following the same reference tracks as its predecessors with a 10-day repeat period. In this study, we use the

Jason-2 SGDR (product version "T"), which contains 20-Hz 104-sample waveform data, from cycles 7–34 (September 2008–June 2009). The geophysical corrections (solid Earth and pole tides, and inverted barometer) and dry troposphere correction have been applied. The wet troposphere correction using the water vapor estimates from the onboard Jason-2 Advanced Microwave Radiometer (AMR) is degraded over the coastal ocean owing to land contamination despite AMR's enhanced spatial resolution (∼26 km) compared to those of TOPEX and Jason-1 (∼50 km) (Brown 2008). The wet troposphere correction calculated from the European Center for Medium Range Weather Forecasts (ECMWF) numerical weather prediction model is thus used. The ionosphere correction derived from Global Ionosphere Map (GIM) is used instead of the correction based on the dual-frequency range measurements also because of land contaminations. The instrument corrections already have been applied to the range measurements in the (S)GDR. No editing criteria related to the Ku band range measurements recommended in the Jason-2 (S)GDR handbook (OSTM 2009) are used in this study because examining the quality of the ocean-retracked SSHs and their potential improvement is one of the objectives of this study.

Figure 1 shows the study area with Jason-2 ground tracks over the California coastal ocean. We investigate the Ku-band radar waveforms along four ascending passes (69, 145, 221, and 43) in this study. The background is the geoid computed using Earth Gravitational Model 2008 (EGM08) (Pavlis et al. 2008), which is used as a reference to assess the

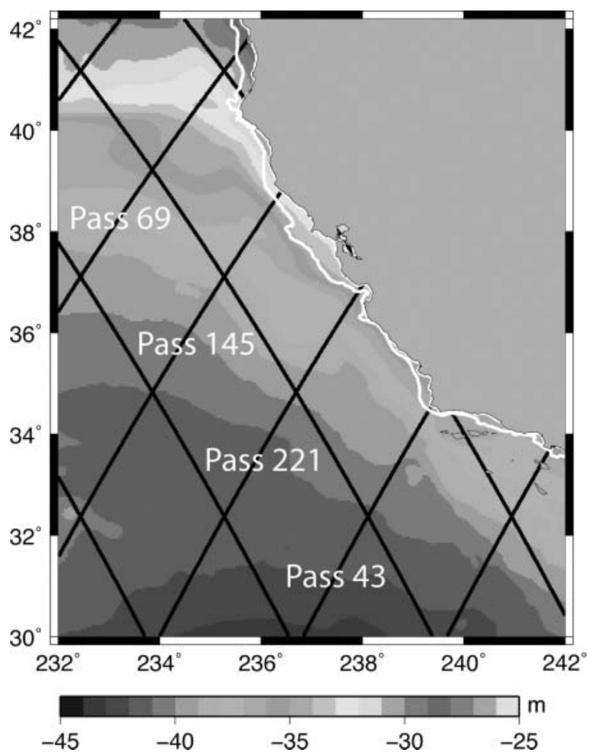

Figure 1. Jason-2 passes over the study region. Ascending passes 69, 145, 221, and 43 (from ocean to land) are examined in this study. Background is the geoids from EGM08, and the white line along the coast indicates the contour of ocean depth 200 m.

performance of the retrackers. The white line along the coast represents a contour of ocean depth 200 m from ETOPO2 (Earth Topography).

3. Waveform Retracking

The radar altimeter waveforms provide the range between the satellite and the surface at nadir via two-way travel time of the transmitted pulse, the Significant Wave Height (SWH) via the slope of the waveform leading edge, and the backscattering coefficients which represent the surface roughness and characteristics via the returned power. The shape of the waveform from incoherent surface scattering can be described based on physical optics theory, which treats the surface as a set of specular points with a given height and slope probability density distribution. The time series of the mean returned power; that is, the waveform, $P(t)$, is represented by the convolution of the instrument point target response (PTR) $\chi(t)$, the impulse response from a smooth sphere (the mean Earth) $S(t)$, and the probability density function (PDF) of the specular points $f_{sp}(t)$ (Brown 1977; Hayne 1980; Barrick and Lipa 1985; Rodriguez 1988) such as:

$$P(t) = S(t) \otimes \chi(t) \otimes f_{sp}(t) \tag{1}$$

The time t is the time measured at the satellite such that $t = 0$ corresponds to the first arrival time of an impulse from the mean ocean surface. To provide a simplified analytical expression, Brown (1977) proceeded with the assumptions that are inherent in the convolution model of near normal incidence rough surface backscatter. These assumptions are generally satisfied over ocean surfaces.

Over ocean surfaces, altimeter retracking algorithms aim to retrieve more accurate estimates of range and SWH, as well as additional parameters such as antenna off-nadir angle and skewness of the surface elevation distribution. Ocean waveform retracking is based upon the convolution representation of the waveform. Therefore, one can recover the specular point PDF by performing a deconvolution of the return radar waveform (Barrick and Lipa 1985; Rodriguez and Chapman 1989). In contrast to TOPEX/Poseidon, Jason-2 (and Jason-1) waveforms are retracked on the ground based on the analytical expression (Brown 1977) denoted by Eq. (1), from which the ocean parameters are estimated with higher accuracy using a Maximum Likelihood Estimator (MLE) (e.g., Rodriguez 1988). The ocean-retracked range measurements provided in Jason-2 (S)GDR are estimated from the 4-parameter MLE (MLE-4), which also retrieves the backscattered power, SWH, and the off-nadir angle (OSTM 2009). The ocean-retracked parameters including the altimeter range can be obtained from Jason-2 (S)GDR products. In addition, the (S)GDR also provides the altimeter range from the ice retracking method, which is also used in this study. The ice retracker is essentially 30% threshold retracker using the mean power of the waveform calculated using Offset Center of Gravity (OCOG) (Bamber 1994) retracking algorithm (P. Thibaut, personal communication, 2010).

In this study, we retrack Jason-2 waveforms using the threshold and modified threshold methods. The description of the threshold method can be found in Davis (1997) and Deng and Featherstone (2006). The modified threshold retracker (Lee et al. 2008b) was originally developed for reprocessing land waveforms from TOPEX/Poseidon to estimate the vertical crustal motion. Over topographic surfaces, it is common to observe a preleading edge bump and a spike after the leading edge. These can lead to erroneous estimates of the retracked range. This is especially the case when using the threshold retracker, which estimates the retracked gate based on the thermal noise and maximum value of the waveform. The

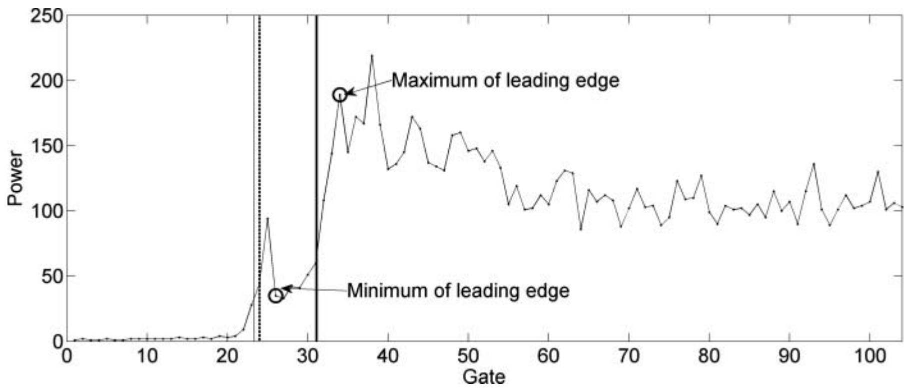

Figure 2. Comparison of retracked gates using ice (thin solid line), threshold 20% (dashed line), and modified 20% threshold (thick solid line) retrackers from a waveform with pre-leading edge bump. The minimum and maximum powers of the leading edge, estimated from the modified threshold retracker, are also indicated.

modified threshold retracker estimates the minimum and maximum values of the apparent leading edge, which are then used to determine the retracked gate with a given threshold level.

Both threshold and modified threshold retrackers are examined over the study area with 10%, 20%, and 50% threshold levels after several experiments. Figure 2 shows an example of a waveform from cycle 31 pass 69 near the coast with its retracked gates using threshold 20% (dashed line), modified threshold 20% (thick solid line), and ice (thin solid line) retrackers. It is evident that the preleading edge bump and the spike after the leading edge lead to different estimates of the retracking gate from these retrackers. This study investigates how these retrackers, as well as the ocean and ice retrackers, could improve the Jason-2 SSHs. It should be noted that, to avoid confusion, we used the ice retracking algorithm to estimate the corresponding retracked gate shown in Figure 2. However, in the following analysis, we directly use the ice retracked measurements available in the (S)GDR.

4. Results

To assess the performance of the retrackers, standard deviations (SD) of the differences between the geoid and the retracked SSHs are computed along with the improvement percentage (IMP) (Hwang et al. 2006) (see Tables 1 and 2) to see the improvement over the ocean-retracked SSHs such as:

$$\mathrm{IMP} = \frac{\sigma_{ocean} - \sigma_{retracked}}{\sigma_{ocean}} \times 100(\%) \tag{2}$$

where σ_{ocean} and $\sigma_{retracked}$ are the standard deviations of the differences between ocean-retracked SSHs and geoids, and retracked SSHs using the other retrackers and geoids, respectively. The precision of the retracked SSHs is estimated separately over the California shallow (depth $<$ 200 m) and deep (depth $>$ 200 m) oceans using all of the Jason-2 cycles from 7–34 for passes 69, 145, 221, and 43 as summarized in Table 2.

Figure 3 shows examples of the comparison of retracked SSHs using ice, original threshold, modified threshold, and ocean retrackers with respect to the geoid (profiles from

Table 1
Statistics of waveform retracking for Jason-2 data used in Figure 3. The highest IMPs are indicated by bold numbers

	Retrackers	Depth < 200 m SD (m)	Depth < 200 m IMP (%)
Cycle 13 Pass 69	Ocean	0.255	—
	Ice	0.180	29.4
	Threshold 10%	0.214	16.1
	Threshold 20%	0.186	27.1
	Threshold 50%	0.261	−2.4
	Modified Threshold 10%	0.103	59.6
	Modified Threshold 20%	0.094	**63.1**
	Modified Threshold 50%	0.150	41.2
Cycle 18 Pass 145	Ocean	0.733	—
	Ice	0.118	83.9
	Threshold 10%	0.114	84.4
	Threshold 20%	0.127	82.7
	Threshold 50%	0.281	61.7
	Modified Threshold 10%	0.093	**87.3**
	Modified Threshold 20%	0.096	86.9
	Modified Threshold 50%	0.134	81.7
Cycle 9 Pass 221	Ocean	0.450	—
	Ice	0.091	79.8
	Threshold 10%	0.105	76.7
	Threshold 20%	0.103	77.1
	Threshold 50%	0.200	55.6
	Modified Threshold 10%	0.071	84.2
	Modified Threshold 20%	0.063	**86.0**
	Modified Threshold 50%	0.130	71.1
Cycle 32 Pass 43	Ocean	0.111	—
	Ice	0.226	−103.6
	Threshold 10%	0.221	−99.1
	Threshold 20%	0.228	−105.4
	Threshold 50%	0.135	−21.6
	Modified Threshold 10%	0.121	−9.0
	Modified Threshold 20%	0.064	**42.3**
	Modified Threshold 50%	0.134	−20.7

top to bottom in the figure) near the coast. It is clear that the ocean-retracked SSHs are generally unreliable and suffer from data loss when getting close to the coast. This is expected because the shape of the waveforms near the coast does not agree with the Brown ocean model, as can be seen from Figure 2, which is represented with a single sharp leading edge with slowly decaying trailing edge. These examples show that the modified threshold retracker can provide improved results in terms of the IMPs as summarized in Table 1 over the shallow ocean. Figure 3 also indicates that the threshold- and ice-retracked SSHs

Table 2
Statistics of waveform retracking from Jason-2 cycles 7–34. The highest IMPs are indicated by bold numbers

	Retrackers	Depth < 200 m SD[1] (m)	IMP[1] (%)	SD[2] (m)	Depth > 200 m SD[1] (m)	IMP[1] (%)	SD[2] (m)
Pass 69	Ocean	1.378	—	1.491	0.821	—	0.814
	Ice	0.777	43.6	0.501	0.731	**11.0**	0.736
	Threshold 10%	1.012	26.6	0.491	0.778	5.2	0.793
	Threshold 20%	0.779	43.5	0.512	0.744	9.3	0.751
	Threshold 50%	1.034	24.9	1.090	0.960	−17.0	0.939
	Modified Threshold 10%	0.526	61.8	0.500	0.806	1.7	0.823
	Modified Threshold 20%	0.517	**62.5**	0.510	0.774	5.6	0.785
	Modified Threshold 50%	0.825	40.1	0.806	0.970	−18.2	0.957
Pass 145	Ocean	1.510	—	1.600	0.768	—	0.758
	Ice	0.491	**67.5**	0.475	0.702	**8.6**	0.715
	Threshold 10%	0.543	64.0	0.543	0.745	3.0	0.791
	Threshold 20%	0.547	63.8	0.537	0.720	6.2	0.734
	Threshold 50%	1.010	33.1	1.518	0.933	−21.5	0.923
	Modified Threshold 10%	0.518	65.7	0.603	0.776	−0.10	0.839
	Modified Threshold 20%	0.521	65.5	0.603	0.750	2.4	0.767
	Modified Threshold 50%	0.762	49.5	0.828	0.948	−23.4	0.941
Pass 221	Ocean	3.458	—	4.548	0.817	—	0.828
	Ice	0.505	85.4	0.537	0.777	**4.8**	0.794
	Threshold 10%	0.542	84.3	0.570	0.865	−5.9	0.892
	Threshold 20%	0.557	83.9	0.577	0.796	2.6	0.814
	Threshold 50%	1.870	45.9	4.210	0.926	2.3	0.929
	Modified Threshold 10%	0.432	87.5	1.096	0.892	−9.2	0.923
	Modified Threshold 20%	0.407	**88.2**	0.478	0.822	−0.6	0.847
	Modified Threshold 50%	0.716	79.3	0.822	0.927	−13.4	0.934
Pass 43	Ocean	0.903	—	0.470	0.680	—	0.679
	Ice	0.571	36.8	0.352	0.631	**7.2**	0.648
	Threshold 10%	0.600	33.6	0.328	0.681	−0.2	0.705
	Threshold 20%	0.595	34.1	0.380	0.652	4.1	0.668
	Threshold 50%	0.994	−10.1	0.709	0.850	−25.1	0.848
	Modified Threshold 10%	0.481	**46.7**	0.355	0.709	−4.3	0.735
	Modified Threshold 20%	0.513	43.2	0.403	0.682	−0.33	0.701
	Modified Threshold 50%	0.840	6.9	0.696	0.866	−27.4	0.869

SD[1] and IMP[1]: without SSB correction.
SD[2]: with SSB correction.

are more precise in coastal regions beyond 2–5 km from the shore in general, while the ocean-retracked SSH is reliable only beyond 10 km. However, as will be shown later, the ocean-retracked SSHs from some of the Jason-2 cycles are noisy even over the deep ocean. As can be seen from Table 2, the modified threshold retrackers with 10% or 20% levels outperform the other retrackers over the shallow ocean except for pass 145. When compared

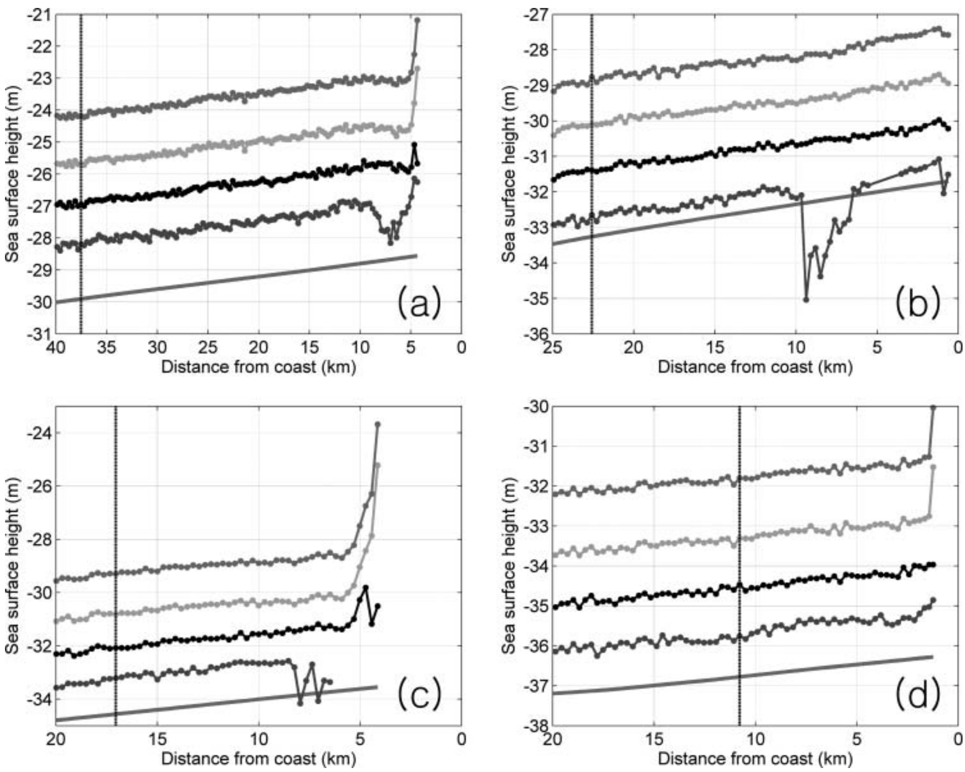

Figure 3. Comparison of retracked SSHs using ice, original threshold, modified threshold, and ocean retrackers with respect to the geoid (profiles from top to bottom) near the coastline from **(a)** cycle 13 pass 69, **(b)** cycle 18 pass 145, **(c)** cycle 9 pass 221, and **(d)** cycle 32 pass 43. 10% threshold level is used for (b), and 20% is used for the others. Vertical dashed lines indicate the location where the ocean depth is 200 m. Arbitrary constants are added for visual clarity.

to the other retrackers, SSHs retracked by the 50% threshold retracker show less significant improvement (averaged IMP $= \sim 23\%$) in the shallow ocean and even no improvement (averaged IMP $= \sim -15\%$) over the deep ocean.

Figure 4 shows the retracked SSH profiles over the entire study area, including the deep ocean from (a) cycle 34 pass 69, (b) cycle 33 pass 145, (c) cycle 13 pass 221, and (d) cycle 20 pass 43 as examples of noisy ocean-retracked SSHs. It can be seen that the ocean retracker is less robust compared to the other retrackers along these passes, even several hundreds of kilometers away from the shore. These noisy ocean-retracked SSHs are found from cycles 7, 8, 17, 20, 23, 24, 26, 30, and 34 for pass 69, cycles 7, 33, and 34 for pass 145, cycles 13, 15, and 33 for pass 221, and cycles 20, 32, 33, and 34 for pass 43 over the deep ocean. It should be noted that these noisy ocean-retracked SSHs are mostly to be flagged based on the editing criteria ("range_rms_ku" or "alt_echo_type") as suggested by the Jason-2 (S)GDR handbook. The black rectangles in Figure 4 indicate the ocean-retracked SSHs that are to be edited out because their corresponding range_rms_ku values are larger than 0.2 m. The ocean retracker was found to perform the best for all the other cycles for each pass over the deep ocean.

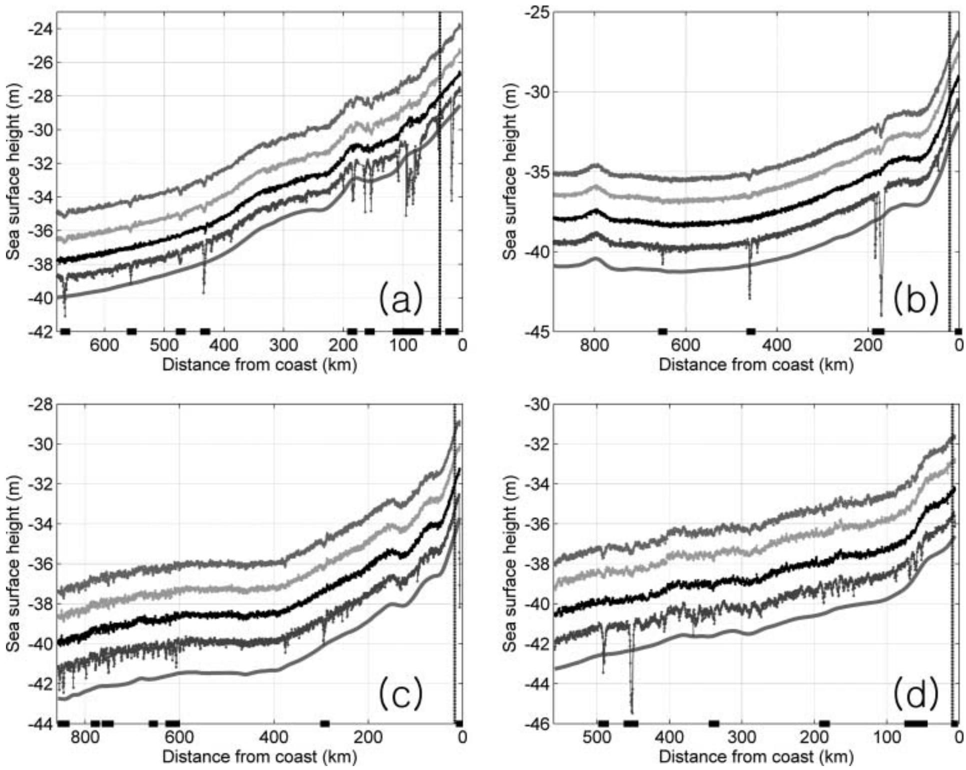

Figure 4. Comparison of retracked SSHs using ice, original threshold, modified threshold, and ocean retrackers (profiles from top to bottom) from **(a)** cycle 34 pass 69, **(b)** cycle 33 pass 145, **(c)** cycle 13 pass 221, and **(d)** cycle 20 pass 43. 20% threshold level is used for (a), and 10% is used for the others. The thick solid line represents the geoids. Vertical dashed lines indicate the location where the ocean depth is 200 m. Black rectangles indicate the ocean-retracked SSHs that are to be flagged based on the editing criteria (range_rms_ku > 0.2 m). Arbitrary constants are added for visual clarity.

We further investigate the waveform shapes along these individual tracks. It is found that the problem of noisy ocean-retracked SSHs comes from the waveforms, as can be seen, as an example, in Figure 5 that illustrates the waveforms from cycle 34 pass 69. It can be seen from Figure 5(a) that some of the waveforms do not show distinct leading edge around the tracking gate 32. Examples of those waveforms in Figure 5(b) differ considerably from the ocean waveforms. They have a noisy leading edge or increasing returned power after the leading edge, which persists until around gates 70–80. Hence, these waveforms do not conform to the Brown ocean model in Eq. (1), which is the physical basis for the ocean retracking algorithm, thus causing the erroneous SSH estimates.

As can be seen from Table 2, over the deep ocean, ice-retracked SSHs show improvement (averaged IMP = ∼8%) over the ocean-retracked SSHs in average using cycles 7–34, while the other retrackers do not generally improve the precision of SSHs. This suggests that careful retracking of Jason-2 waveforms also has a potential, even over the deep ocean, to improve noisy SSHs which are to be edited out.

The results above are generated without applying the sea state bias (SSB) correction because only the SSB correction empirically determined from SWH and wind speeds (Labroue et al. 2004), which are presumably based on ocean-retracked parameters, is

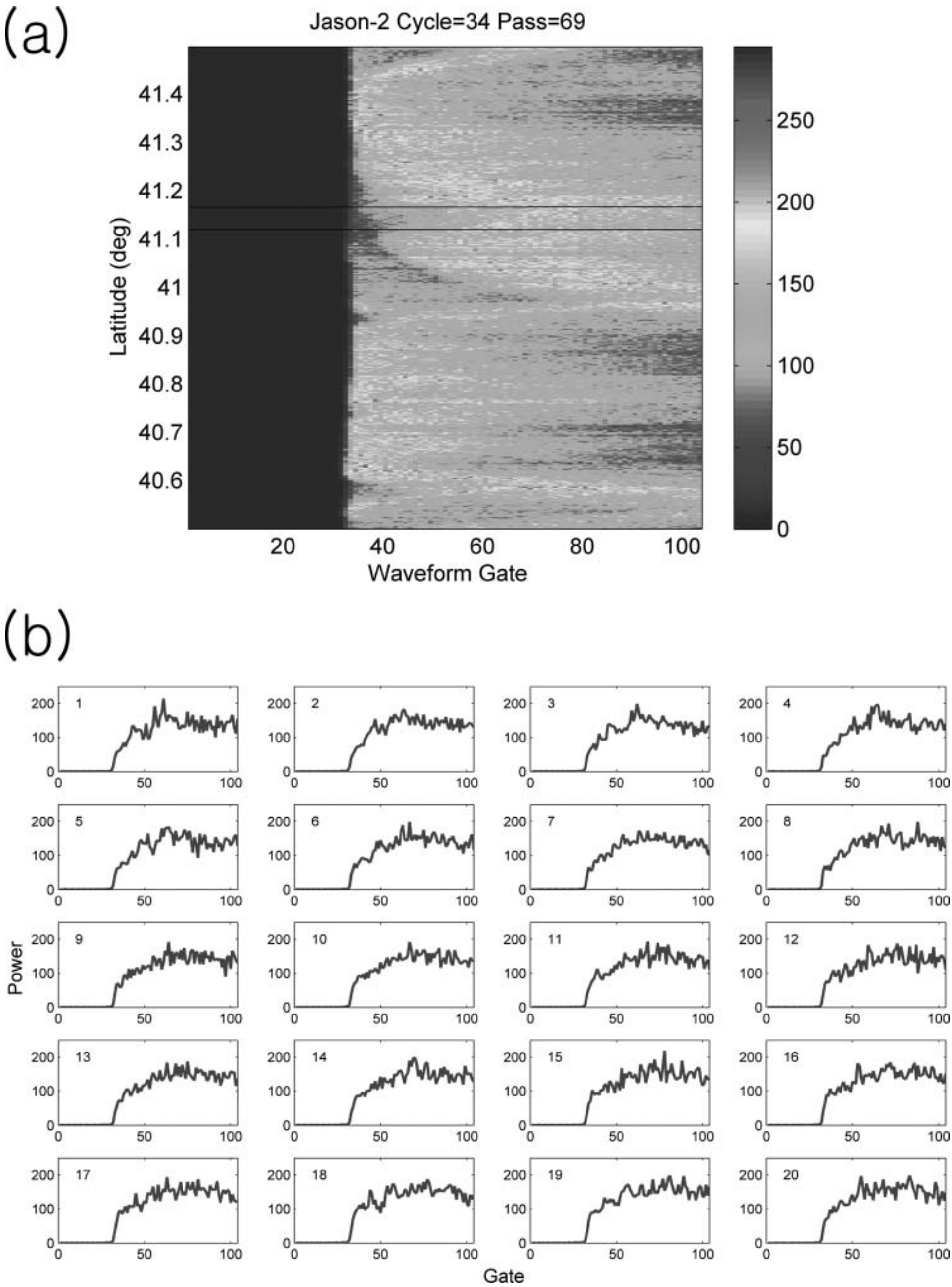

Figure 5. **(a)** Waveforms from cycle 34 pass 69; **(b)** waveforms over the region indicated with a black box in (a). The waveform sequence, numbered from 1 to 20, follows the satellite flight direction.

provided in Jason-2 (S)GDR. The SSB correction over the coastal ocean can thus introduce additional error. Moreover, it is expected that the SSB correction based on ocean-retracked parameters is not adequate for other retracked range measurements, which can be more precise, as shown above, even over the deep ocean. In Table 2, additional SDs of the differences between the geoid and the retracked SSHs with the SSB correction are shown. Over the shallow ocean, as expected, except for pass 43, the precision of ocean-retracked measurements deteriorate after the SSB correction. It is observed that, over the deep ocean, the precision of the ocean-retracked measurements improves after the SSB correction except for pass 221. Furthermore, the SSB corrections to other retracked SSHs over the deep ocean again generally deteriorate the precision as expected. These results suggest that more adequate SSB corrections are needed over the shallow ocean and even over the deep ocean when the ocean retracker is outperformed by the other retrackers.

5. Discussions, Conclusions and Future Studies

In this study, we evaluated Jason-2 SSHs retracked by the ocean, ice, original threshold, and modified threshold retrackers over the California coastal ocean attempting to extract precise SSHs from both land-contaminated and ocean-dynamics distorted coastal radar altimeter waveforms. The performance of these retrackers is examined by comparing EGM08 geoids with retracked SSHs assuming that the retracked SSHs should be as smooth as the geoid profile. Over the shallow ocean, the modified threshold retracker outperforms the other retrackers by providing more precise SSHs beyond 2–5 km from the coastline. This may also indicate the capability of Jason-2 to retrieve more precise SSHs closest to the coastline compared to TOPEX (Brooks et al. 1997) or ERS-2 (Deng and Featherstone 2006). Over the deep ocean, the ocean retracker used in (S)GDR is less robust in estimating precise SSHs for some cycles due to the waveforms not conforming to the Brown ocean model. Those noisy ocean-retracked SSHs are recommended to be flagged according to the editing criteria in the Jason-2 (S)GDR handbook (OSTM 2009). However, the retrackers developed for nonocean surfaces are tested to check if they can improve the SSH precision over the deep ocean. It is found that the ice retracker outperforms the ocean retracker when the return waveforms do not conform to the Brown model.

Since the goal of retracking waveforms is to provide higher spatial resolution (~350 m), the current geoid model may not be an adequate reference “truth” to judge the methods with absolute accuracy. For a future study, we will investigate the possibility of independently validating the retracked data using synthetic SSHs derived from satellite imagery, coastal high-frequency (HF) radars, and tide gauges. The synthetic heights can be derived from surface geostrophic currents computed by applying the Maximum Cross Correlation (MCC) method to sequential thermal infrared (AVHRR) and ocean color (MODIS, SeaWiFS) satellite imagery (Bowen et al. 2002; Crocker et al. 2007). In addition, we will use high-resolution coastal HF radars to compute space/time coastal current fields that can be inverted to generate synthetic SSH fields.

Finally, the SSB corrections appropriate for other retrackers are suggested to be developed either empirically or physically. Investigating hydrodynamic and electromagnetic models to understand the physical behaviors of the SSB is of particular interest.

Acknowledgements

This research is supported by grants from NASA’s Ocean Surface Topography Science Team Program, and from the Ohio State University’s Climate, Water, and Carbon Program. We also thank two anonymous reviewers for their constructive comments.

References

Anzenhofer, M., C. K. Shum, and M. Rentsh. 1999. Coastal altimetry and applications. Geodetic Science Report 464. Ohio State University, Columbus, Ohio, USA.

Bamber, J. L. 1994. Ice sheet altimeter processing scheme. *Int. J. Remote Sens.* 15:925–938.

Bao, L., Y. Lu, and Y. Wang. 2009. Improved retracking algorithm for oceanic altimeter waveforms. *Prog. Nat. Sci.* 19:195–203.

Barrick, D. E. and B. J. Lipa. 1985. Analysis and interpretation of altimeter sea echo. *Adv. Geophys.* 27:61–100.

Bowen, M., W. J. Emery, J. L. Wilkin, P. Tildesley, I. J. Barton, and R. Knewtson. 2002. Extracting multi-year surface currents from sequential thermal imagery using the maximum cross correlation technique. *J. Atm. Oceanic Tech.* 19:1665–1676.

Brooks, R. L., D. W. Lockwood, and J. E. Lee. 1997. Land effects on TOPEX radar altimeter measurements on Pacific Rim coastal zones. NASA WFF Publ. http://topex.wff.nasa.gov/documents/7.html

Brown, G. S. 1977. The average impulse response of a rough surface and its applications. *IEEE Trans. Antennas Propag.* 25:67–74.

Brown, S. 2008. Jason-2 wet tropospheric coastal performance. Coastal Altimetry Workshop, February 5–7, in Silver Spring, Maryland.

Chelton, D. B., J. C. Ries, B. J. Haines, L.-L. Fu, and P. S. Callahan. 2001. Satellite altimetry. In *Satellite altimetry and earth sciences: A handbook of techniques and applications*, eds. L.-L. Fu and A. Cazenave. New York: Elsevier, pp. 1–132.

Crocker, R. I., W. J. Emery, D. Matthews, and D. Baldwin. 2007. Computing ocean surface currents from infrared and ocean color imagery. *IEEE Trans. Geosci. Remote Sens.* 45:435–447.

Davis, C. H. 1997. A robust threshold retracking algorithm for measuring ice-sheet surface elevation change from satellite radar altimeter. *IEEE Trans. Geosci. Remote Sens.* 35:974–979.

Deng, X., W. E. Featherstone, C. Hwang, and P. A. M. Berry. 2002. Estimation of contamination of ERS-2 and POSEIDON satellite radar altimetry close to the coasts of Australia. *Marine Geodesy* 25:249–271.

Deng, X. and W. E. Featherstone. 2006. A coastal retracking system for satellite radar altimeter waveforms: Application to ERS-2 around Australia. *J. Geophys. Res.* 111, doi: 10.1029/2005JC003039.

ETOPO2v2 Global Gridded 2-minute Database, National Geophysical Data Center, National Oceanic and Atmospheric Administration, U.S. Dept. of Commerce. Available at http://www.ngdc.noaa.gov/mgg/global/etopo2.html

Gommenginger, C., P. Thibaut, L. Fenoglio-Marc, X. Deng, J. Gomez-Enri, and Y. Gao. 2009. Retracking altimeter waveforms near the coasts. In *Coastal altimetry*, eds. S. Vignudelli, A. Kostianoy, and P. Cipollini. Berlin: Springer.

Hayne, G. S. 1980. Radar altimeter mean return waveform from near-normal-incidence ocean surface scattering. *IEEE Trans. Antennas Propag.* 28:687–692.

Hwang, C., J. Guo, X. Deng, H.-Y. Hsu, and Y. Liu. 2006. Coastal gravity anomalies from retracked Geosat/GM altimetry: Improvement, limitation and the role of airborne gravity data. *J. Geod.* 80:204–216.

Labroue, S., P. Gaspar, J. Dorandeu, O. Z. Zanife, F. Mertz, P. Vincent, and D. Choquet. 2004. Nonparametric estimates of the sea state bias for the Jason-1 radar altimeter. *Marine Geodesy* 27:453–481.

Lee, H., C. K. Shum, C. Y. Kuo, Y. Yi, and A. Braun. 2008a. Application of TOPEX altimetry for solid earth deformation studies. *Terr. Atmos. Ocean. Sci.* 19:38–46.

Lee, H., C. K. Shum, Y. Yi, A. Braun, and C.-Y. Kuo. 2008b. Laurentia crustal motion observed using TOPEX/POSEIDON radar altimetry. *J. Geodyn.* 46:182–193.

Martin, T. V., H. J. Zwally, A. C. Brenner, and R. A. Bindschadler. 1983. Analysis and retracking of continental ice sheet radar altimeter waveforms. *J. Geophys. Res.* 88:1608–1616.

OSTM/Jason-2 Products Handbook. 2009. JPL, OSTM-29-1237.

Pavlis, N. K., S. A. Holmes, S. C. Kenyon, and J. K. Factor. 2008, April. An earth gravitational model to degree 2160: EGM2008. Vienna, Austria: EGU-2008. http://earth-info.nga.mil/GrandG/wgs84/gravitymod/egm2008/index.html

Rodriguez, E. 1988. Altimetry for non-Gaussian oceans: Height biases and estimation of parameters. *J. Geophys. Res.* 93:14107–14120.

Rodriguez, E. and B. Chapman. 1989. Extracting ocean surface information from altimeter returns: The deconvolution method. *J. Geophys. Res.* 94:9761–9778.

Shum, C. K., Y. Yi, K. C. Cheng, C. Y. Kuo, A. Braun, S. Calmant, and D. P. Chambers. 2003. Calibration of Jason-1 altimeter over Lake Erie. *Marine Geodesy* 26:335–354.